MOX-Report No. 68/2017

3D physics-based numerical simulations: advantages and current limitations of a new frontier to earthquake ground motion prediction. The Istanbul case study.

Paolucci, R.; Infantino, M.; Mazzieri, I.; Özcebe, A.G.;

Smerzini, C.; Stupazzini, M.

MOX, Dipartimento di Matematica
Politecnico di Milano, Via Bonardi 9 - 20133 Milano (Italy)

mox-dmat@polimi.it http://mox.polimi.it

3D physics-based numerical simulations: advantages and current limitations of a new frontier to earthquake ground motion prediction. The Istanbul case study.

Roberto Paolucci[1], Maria Infantino[1], Ilario Mazzieri[2], Ali Güney Özcebe[1], Chiara Smerzini[1], Marco Stupazzini[3]

[1] Dept. of Civil and Environmental Engineering, Politecnico di Milano, Italy

[2] Dept. of Mathematics, Politecnico di Milano, Italy

[3] MunichRe, Munich, Germany

Abstract In this paper, an overview is presented to motivate the use of 3D physics-based numerical simulations of seismic wave propagation to support enhanced Probabilistic Seismic Hazard Assessment. With reference to the case study of Istanbul, we introduce the activities required to construct a numerical model of the surface geology and topography and to determine the input conditions to trigger future earthquakes in a physically sound way. Owing to the intrinsic frequency limitations of the numerical simulations, a post-processing technique to produce realistic broadband waveforms is introduced, allowing to correlate short-period to long-period spectral ordinates from an Artificial Neural Network. Finally, the results obtained in Istanbul from numerous physics-based ground motion scenarios of M7+ earthquakes allow us to throw light on the potential added value to PSHA of the 3D numerical simulations. Namely, to provide locally constrained probabilistic distributions of ground motion intensity measures, matching the actual footprint of a large earthquake in the specific area under study.

Introduction

Empirical ground motion prediction equations (GMPE) and 3D physics-based numerical simulations (3DPBNS) are generally presented as alternative tools for earthquake ground motion prediction and for its application to seismic hazard assessment studies. While the use of GMPEs is well consolidated, in the framework of both probabilistic and deterministic studies, 3DPBNS seem to be still confined to a relatively restricted range of applications, where earthquake ground motion scenarios are produced in an almost deterministic way.

Such dichotomy is obstructive and does not allow to fully exploit those techniques, shading lights on their limitations on one hand and, on the other hand, on

their potential advantages to produce more reliable results, as summarized in Table 1. More specifically, the limitation of GMPEs not to be sufficiently well calibrated for those conditions, such as large earthquake magnitude, near-source, soft soil sites, complex geological irregularities, that typically govern seismic hazard at a site, decreases the reliability of probabilistic seismic hazard assessment (PSHA) results, typically based on GMPE application as a tool for ground motion prediction. Moreover, 3DPBNS have not been sufficiently developed yet to yield a consensus on the engineering applicability of their broad-band results, also because, in spite of the ongoing progress in the recent years, there are still relatively few cases of fully worked out validation exercises on real earthquake case studies and comparison with records.

Table 1. Advantages and limitations of GMPEs and 3DPBNSs

	PROs	**CONs**
GMPE	- ease-of-use - calibrated on records - adapted to different tectonic environments and site conditions	- lack of records to solve important conditions, such as near-source and complex geological environments - only peak values of motion - recalibration when new data are available - no correlation of ground motion intensities among multiple sites and among different spectral periods
3DPBNS	- flexibility to produce synthetics in arbitrary site and source conditions - parametric analyses allowed - spatial correlation of simulated ground motion - insight into the earthquake physics	- high-frequency computational and modelling limit - high computational costs - need of expert users - hardly available information to construct a reliable 3D model - large epistemic uncertainties - few well documented validation case studies on real earthquakes

In Figure 1, the typical conditions for which GMPEs and 3DPBNSs should be considered in a PSHA study are sketched: on one hand, GMPE provide reliable results when the source-to-site distance is sufficiently large, e.g., at least larger than the size of the fault, and no complex geological conditions are present, while, on the other hand, the vicinity to the source and the complex geological conditions should lead to the selection of 3DPBNS as the main tool for earthquake ground motion prediction.

To capture the potential drawbacks of fully relying on GMPEs for PSHA, typically expressed in terms of uniform hazard spectra at rock sites, it is worth considering Figure 2, where the Peak Ground Acceleration (PGA) values from the NGA 2014 dataset (Ancheta *et al*., 2014) are extracted, for records with magnitude $M >$

6 and R_{JB} (i.e., distance from the surface projection of fault) < 20 km, and plotted as a function of $V_{S,30}$ (i.e., average shear wave velocity in the top 30 meters according to seismic norms). The scarcity of suitable records for rock conditions (e.g., $V_{S,30}$ > 800 m/s) is evident, as well as the consideration that some of such records are obtained in conditions (such as the Pacoima and Lexington dam in Figure 2) far away from the ideal reference free-field rock.

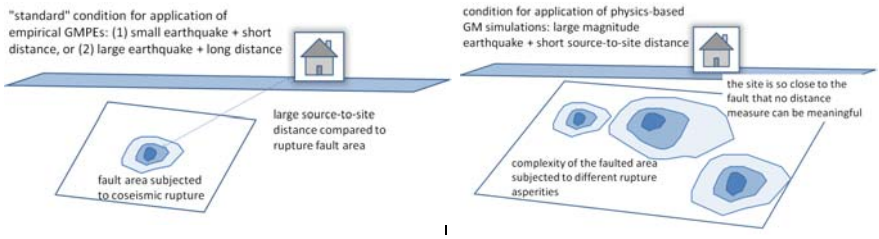

Fig. 1. Sketches for the optimum conditions of applicability of GMPE and 3DPBNS, depending on the distance of the site to the seismic source.

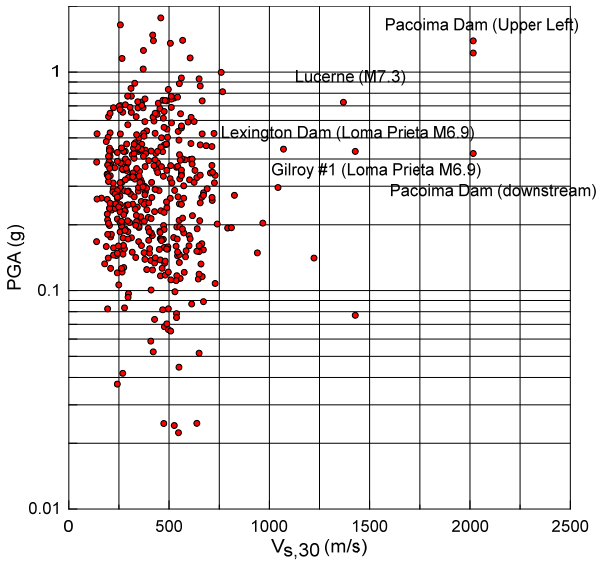

Fig. 2. Selection of earthquake records from the NGA 2014 dataset, with M > 6 and R_{JB} < 20 km, as a function of $V_{S,30}$. Some of the stations corresponding to "rock" conditions are denoted.

The Marmara Sea region is an ideal area were the potential advantages and limitations of GMPEs and 3DPBNSs can be tested, because of coupling the high seismic hazard related to the major seismic gap on the North Anatolian Fault, expected to produce Magnitude 7+ earthquakes (for a comprehensive review see,

among many others, Bohnhoff *et al*., 2013; Akinci *et al*., 2017; Aochi *et al*., 2017), with the huge seismic risk exposure of Istanbul.

In this paper, we aim at introducing the complete workflow of a PSHA study carried out in Istanbul, in the framework of updating the seismic hazard model for reinsurance purposes, where results of a comprehensive set of 3DPBNS were exploited to provide an enhanced seismic hazard assessment. This paper provides an overview of such study, regarding in particular:

1) construction of the numerical model for 3DPBNS;
2) simulations of different ground motion scenarios by generating realistic fault-slip distributions for different scenario earthquakes;
3) construction of broad-band synthetics through an Artificial Neural Network-based procedure;
4) input of the 3DPBNS results into a PSHA framework.

The simulations were carried out using the numerical code SPEED (http://speed.mox.polimi.it/), designed for the seismic wave propagation analysis in large areas, including the coupled effects of a seismic fault rupture, the propagation path through Earth's layers, localized geological irregularities, such as alluvial basins, and soil-structure interaction problems. Based on a discontinuous version of the classical spectral element method introduced by Faccioli *et al*. (1997), SPEED (Mazzieri *et al*., 2013) is naturally oriented to solve multi-scale numerical problems, allowing one to use non-conforming meshes (*h*-adaptivity) and different polynomial approximation degrees (*N*-adaptivity) in the numerical model. By taking advantage of the hybrid MPI-OpenMP parallel programming SPEED runs on multi-core computers and large clusters (e.g., Marconi at CINECA, https://www.cineca.it/en/content/marconi).

SPEED was successfully verified within the Grenoble benchmark (Stupazzini *et al*., 2009; Chaljub *et al*., 2010), validated by comparison with several among the most recent worldwide earthquakes, including L'Aquila 2009, M_w6.3 (Smerzini and Villani, 2012; Evangelista *et al*., 2017), Chile 2010, M_w 5.2 (Pilz *et al*., 2011), Christchurch 2011, M_w6.2 (Guidotti *et al*., 2011), Emilia 2012, M_w 6.0 (Paolucci *et al*., 2015), and also applied to simulate devastating earthquakes of the past, such as the Marsica 1915, M_w6.7 (Paolucci *et al*., 2016). A repository of results of the 3DPBNS carried out by SPEED can be consulted at the web site http://speed.mox.polimi.it/.

From the tectonic and geological framework to the 3D spectral element model

Leaving details to Infantino (2016), we summarize here the main input data required and how they are cast into a 3D numerical model, with reference to the Istanbul case.

3D geological model

First, a geological model has been constructed, based on collection of the following data:

- digital elevation model and bathymetry, see Figure 3a;
- crustal structure, typically in form of a layered model of S and P wave velocity, V_S and V_P;
- local shallow geological structure, typically in the form of a spatial model of V_S and V_P, variable both in the horizontal and vertical direction, and possibly including the corresponding models for internal soil damping and local variation of shear modulus and damping as a function of shear strain (or, in 3D, of the second invariant of the strain tensor).

Information of the local shallow geology structure is by far the most difficult to gather in a format suitable for the 3D numerical modelling of the area. However, it should be kept in mind that the level of detail of input data should be balanced with the actual computer power limitations: on the one hand, it is useless to get small-scale details on the local geology, when the numerical mesh is bounded to resolve up to, say, 2 Hz, in order to make the number of degrees-of-freedom and the computer time affordable. On the other hand, even with unlimited computational resources, a detailed in-field survey on a vast area is very seldom available. For this reason, extending the frequency limit of 3DPBNSs beyond about 2 Hz is nowadays practically meaningless, unless focus is limited to predicting ground motions at rock or stiff soil sites.

For the Istanbul case, according to the geotechnical site characterization provided by Özgül (2011), the following procedure has been adopted to define the 3D soil model. First, the maps presented by Özgül (2011) have been digitized to obtain the distribution of $V_{S,30}$ and rock/soil classification for the whole Istanbul region. Second, by making use of three sets of data, namely, $V_{S,30}$, rock/soil map and slope information, six site classes have been assigned ranging from $V_{S,30}$ = 250 m/s to $V_{S,30}$ = 1350 m/s, see Figure 3b and, for each class, a V_S profile has been considered, as shown in Figure 3c.

Although a non-linear visco-elastic model is available in SPEED, as introduced by Stupazzini *et al*. (2009), this was not used in the present numerical simulations, and results presented in this work refer to the linear visco-elastic case, where quality factor correlation of ground motion intensities among multiple sites and among different spectral periods is not accounted for.

The seismic source model

The second set of input data refers to the seismic source model. Two basic families of models exist: (1) dynamic source models, where rupture is initiated by specifying a stress perturbation within a given, more or less irregular, area of the fault to reach a yield condition and introducing suitable friction relationships be-

tween stress and the resulting fault slip (Madariaga and Olsen, 2002); (2) kinematic source models, where a more or less heterogenous distribution of co-seismic slip is applied along the fault, together with a slip source function, typically in the form of a sigmoid function, with initiation time and length depending on the local rupture velocity and rise-time, respectively. As shown in Figure 4, a kinematic source model, requires to input, on each node of the fault plane, both the mechanical properties of the fault material (e.g. shear modulus) and the kinematic properties for the characterization of the space-time evolution of seismic slip.

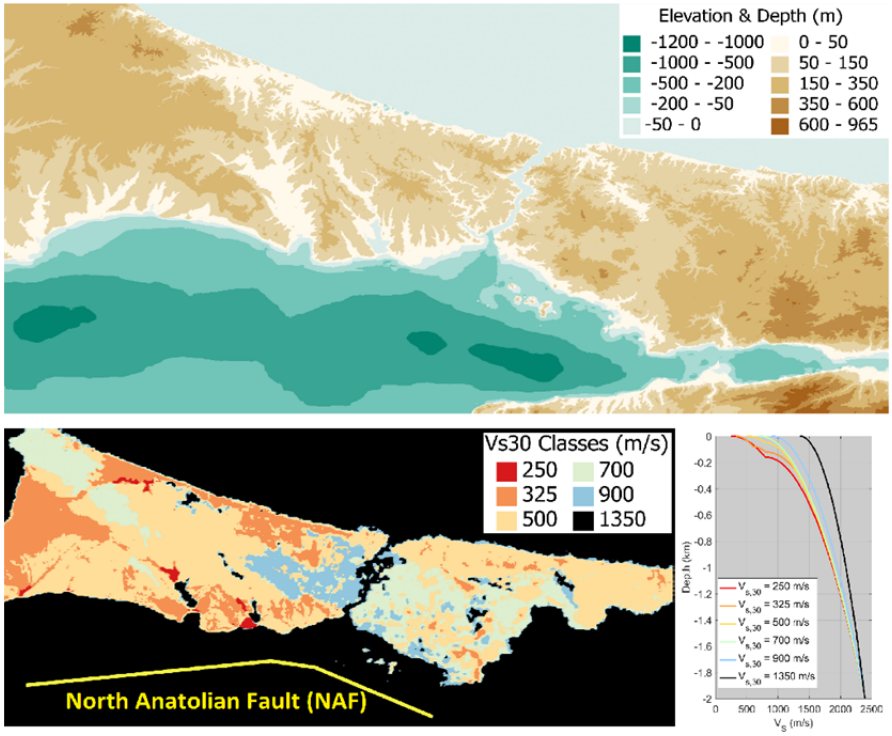

Fig. 3. Top: bathymetry and digital elevation model of the Marmara Sea area adopted in SPEED. Bottom: map of classes of $V_{S,30}$ based on Özgül (2011) and simplified velocity profiles for each $V_{S,30}$ class, adopted in SPEED.

The kinematic approach is preferred in most engineering applications of 3DPBNS, because it complies with the following key features:

- it is cost-effective, i.e., it does not imply a significant increase of the computer time;
- it can be adapted to model effectively not only the low-frequency, but also the high-frequency seismic energy radiation.

The latter feature requires the spatial slip distribution along the fault, as well as the other fault parameters, such as the rise time, the peak time of the slip, the rupture velocity, to fulfill spatial correlation constraints derived from dynamic rupture simulations (see e.g., Mai and Beroza, 2003; Gallovič and Brokešová, 2004; Causse *et al*., 2009). In the SPEED code, the kinematic approaches proposed by Herrero and Bernard (1994) and by Crempien and Archuleta (2015) were implemented. In the first one, the heterogeneities of the slip distribution are assumed to present a k^{-2} spectral decay in the wavenumber domain, leading to the Brune (1970) spectrum ω^{-2} fall-off in the frequency domain, while in the second one a comprehensive recipe was proposed for broadband seismograms generation based on correlation of fault parameters, complying with the SCEC validation criteria (Goulet *et al*., 2015).

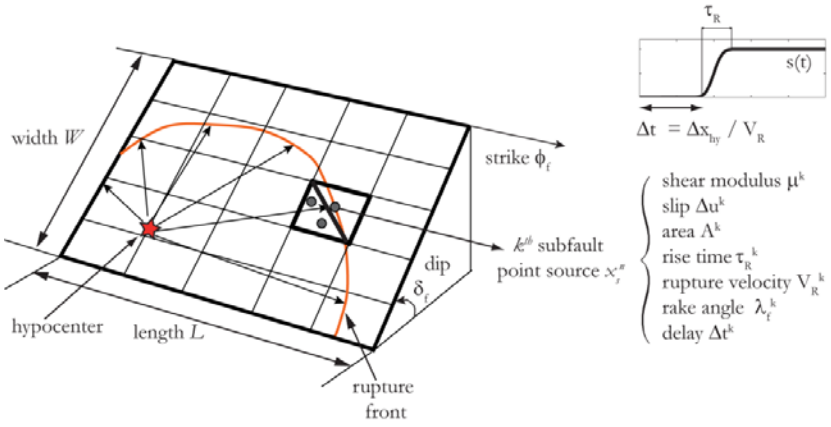

Fig. 4. Sketch of kinematic numerical modeling of an extended seismic source.

Both kinematic approaches mentioned above are then suitable to generate broadband input motions for future earthquakes with prescribed Magnitude along a given fault, by setting random variability of the fault parameters. In Figure 5, the sketch of the Marmara Sea area under study is provided, together with the North Anatolian Fault (NAF) segmentation and the slip distribution models for the sample M_w7 scenario earthquakes considered in the following. Three modes of fault rupture propagation are selected, with reference to directivity condition with respect to Istanbul: forward (scenario 1), neutral (scenario 2) and backward (scenario 3) directivity.

The SPEED numerical model of the Marmara Sea region

Finally, the information above is condensed into a spectral element numerical model (Figure 6), consisting of more than 2 million hexahedral elements and corresponding, with a spectral degree N=4, to about 500 million degrees of freedom.

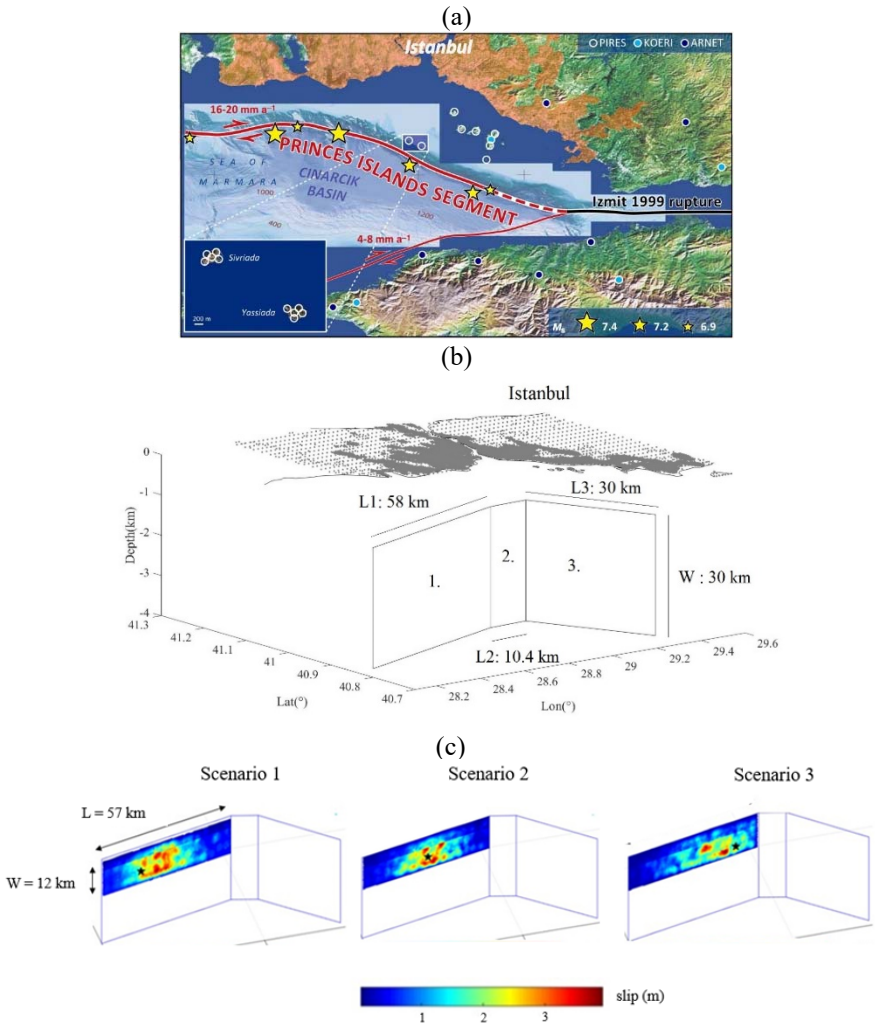

Fig. 5. (a): Tectonic setting of the North Anatolian Fault, reproduced from Bohnoff *et al*. 2013. The fault segment investigated, the bold red line, is the eastern part of the current Marmara seismic gap. The black line marks the observed rupture zone of the 1999 Izmit event, while the dashed red line indicates its potential link with the Princes Islands segment. (b) Geometric scheme of the fault considered in this study and location of Istanbul identified by grey points. (c) Three fault slip distributions generated according to Herrero and Bernard (1994) approach for a Mw 7.0 earthquake scenario and different directivity conditions with respect to Istanbul: forward (scenario 1), neutral (scenario 2) and backward (scenario 3) directivity. The epicenter locations are represented by black stars.

The spectral degree was selected in order for the maximum frequency to be accurately propagated by the numerical integration scheme to be about 1.5 Hz (using

a rule of thumb of about 5 grid points per minimum wavelength in heterogeneous media modelled by spectral elements, according to Faccioli *et al.*, 1997). The runs were carried out at the Fermi supercomputer (now replaced by Marconi) at CINECA, Italy, requiring about 24 h with 8192 cores for simulating T=60 s of wave propagation with a time step Δt = 0.001 s.

Thirty earthquake ground motion scenarios were generated, with M_w ranging from 7.0 to 7.4, by randomly generating the kinematic slip distribution according to either Herrero and Bernard (1994) or Crempien and Archuleta (2015) approaches. For most of M_w7.0 earthquakes, only segment 1 in Figure 5b was activated, while, for all M_w 7.2 and 7.4 earthquakes, rupture extended to the three segments of the NAF facing Istanbul. As shown by Infantino (2016), the convex shape itself of the NAF along the Marmara Sea and its relative position with respect to Istanbul makes it more likely that a directive scenario may occur in the city.

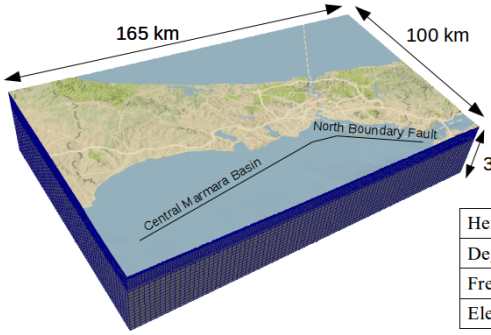

Horizontally stratified crustal model

Depth (km)	V_S (m/s)	Q(-)
0-5	Fig. 3	V_S /10
5-10	3490	350
10-20	3500	350
20-30	3920	400

Computational model

Hexahedral elements	2.257.482
Degrees of freedom	~500 million
Frequency range	0 to 1.5 Hz
Element size range	180 m to 2 km

Fig. 6. Sketch of the SPEED numerical model.

Producing broad-band synthetics from 3DPBNS

One of the main drawbacks of 3DPBNS is that synthetics are reliable only in the long period range, typically above 0.75-1 s, owing to the limitations posed both by computational constraints as well as by lack of detailed data to constrainthe soil model as well the source at high frequency (see overview in Paolucci *et al.*, 2014). On the other hand, earthquake engineering applications need broad-band (referred to as BB hereafter) ground motion time histories with realistic features in a range of frequencies that is broad enough to cover the vibration characteristics of fundamental and higher modes of the structures, say from 0 to 25 Hz.

The most commonly used approach to produce BB waveforms relies on a hybrid modelling which combines in the frequency domain the low-frequency waveforms from 3DPBNS with high-frequency signals from stochastic approaches, based either or point- or finite- source modeling (e.g., Boore, 2003; Motazedian and Atkinson, 2005) or Empirical Green's function (e.g., Kamae *et al.*, 1998; Mai *et al.*, 2010). The main disadvantages of such an approach, especially when applied for hazard assessment at regional scale, are the lack of correlation between the low and high frequency parts of ground motion and the strong impact of the choice of the transition frequency over which the deterministic and stochastic parts of the Fourier spectrum are glued.

In this work, an approach based on Artificial Neural Networks (ANN), referred to as ANN2BB, has been adopted. Referring to Paolucci *et al.* (2017) for a thorough introduction of the method and verification tests against real case studies, we summarize herein its key points. Denoting by T^* the minimum period of the 3DPBNS-based synthetics, the ANN2BB approach consists of the following steps:

a) an ANN is trained based on a strong motion records dataset (namely, SIMBAD, see Smerzini *et al.* 2014), separately for horizontal (geometric mean) and vertical components. The ANN allows to predict short period horizontal/vertical spectral ordinates ($T < T^*$) taking as input the long period ones obtained from the 3DPBNS ($T \geq T^*$);
b) for each simulated waveform, a target ANN2BB response spectrum is generated by application of the previously trained ANN: therefore, the resulting spectrum is equal to that simulated by 3DPBSN at long periods, while at short periods it consists of the ANN outputs;
c) a hybrid 3DPBNS-stochastic modeling is applied to inject high-frequency in the simulated low-frequency waveform and, hence, to make it usable for the following step;
d) finally, the hybrid waveform is iteratively modified in the frequency domain, with no phase change, until its response spectrum matches the target ANN2BB spectrum.

In Paolucci *et al*. (2017) it has been demonstrated by comparison with earthquake observations that this approach allows: (i) to obtain realistic waveforms both in time and frequency domains, in line with earthquake observations; (ii) to predict maps of short-period peak values of ground motion incorporating those effects reproduced by the physics-based simulations, such as source directivity/directionality and complex basin effects; (iii) to preserve the spatial correlation features of ground motion, of particular interest for seismic hazard assessment at regional scale.

The ANN2BB approach was used to process all ground motion scenarios produced by SPEED. In Figure 6 a sample of results is shown, consisting of the NS acceleration (top) and velocity (bottom) time histories at four sites in the Istanbul area, for the 3 selected scenarios (see Figure 5). Realistic time histories can be ap-

preciated, together with the consistency of arrival times and dependency of simulated ground motion on the directivity features of the rupture scenario, with largest values corresponding to Scenario 1, where the largest asperities are aligned along the pathway from the hypocenter to Istanbul.

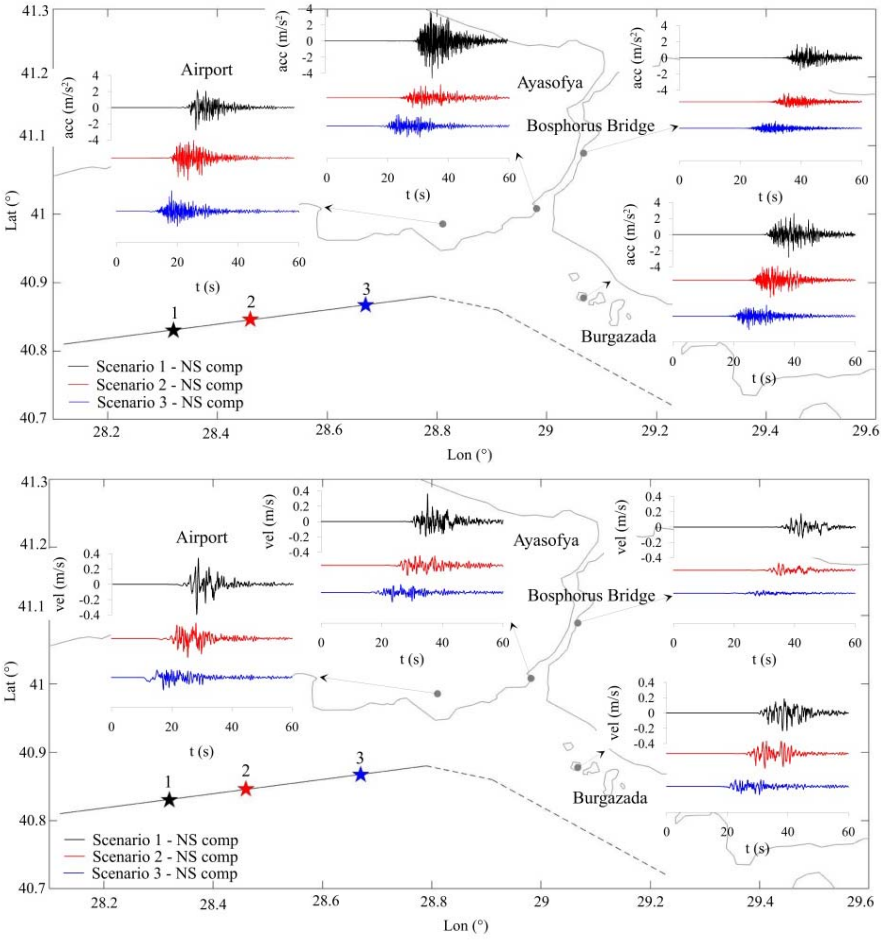

Fig. 7. NS components of acceleration (top) and velocity (bottom) time histories at four sites in Istanbul, obtained with three different earthquake scenarios (1, 2 and 3) of M_w 7.0 identified by different colors. The fault is shown with a continuous black line while the epicenter positions are represented by stars. Slip distributions are illustrated in Figure 4.

In Figure 8, the effect of ANN2BB post-processing is illustrated in detail, with reference to the Scenario 2 synthetics at the Ayasofya site. It is clear that processing enriches the high frequency portion of the waveform, while keeping the

medium-to-low frequency portions practically invariant, as can be seen by the velocity and displacement time histories.

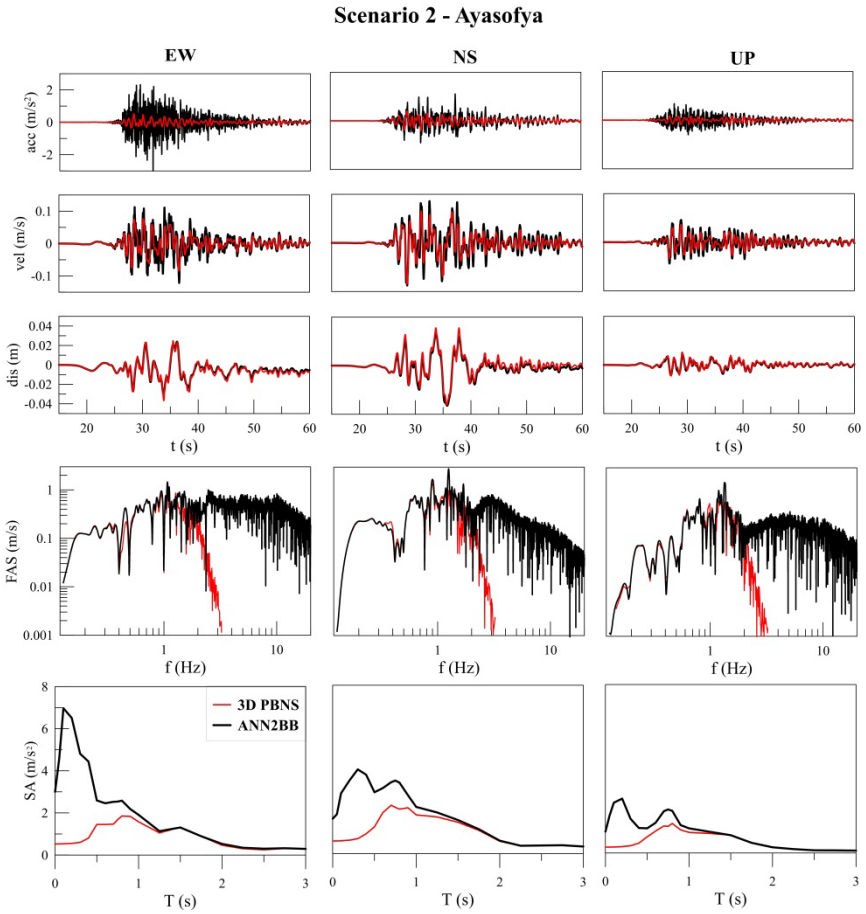

Fig. 8. From top to bottom: acceleration, velocity, displacement time histories, Fourier Amplitude Spectra and Response Spectra for the three components at the site of Ayasofya obtained with the 3D PBNS (thin red line) and ANN2BB (black line) for Scenario 2 (Fig. 5b).

Finally, we show in Figure 9 the maps of horizontal (geometric mean) peak ground velocity (PGV) for the three considered scenarios, together with the median PGV map for the whole set of M_w7 scenarios, as well as the median PGV map according to the GMPE proposed by Cauzzi *et al*. (2015), referred to as CEA15. It can be observed that there is a good agreement in terms of median values provided by the GMPE for the M_w7 scenarios, with the median map approaching the neutral directivity Scenario 2, especially in the western part of Istanbul. It should be noted that, as discussed by Infantino (2016), such agreement is not found any more for those scenarios involving rupture along the three segments of the NAF (M_w7.2 and

7.4), for which only the incorporation of forward directivity effects in GMPEs (such as Bray and Rodriguez-Marek, 2004) can explain the high ground motion values obtained in Istanbul area.

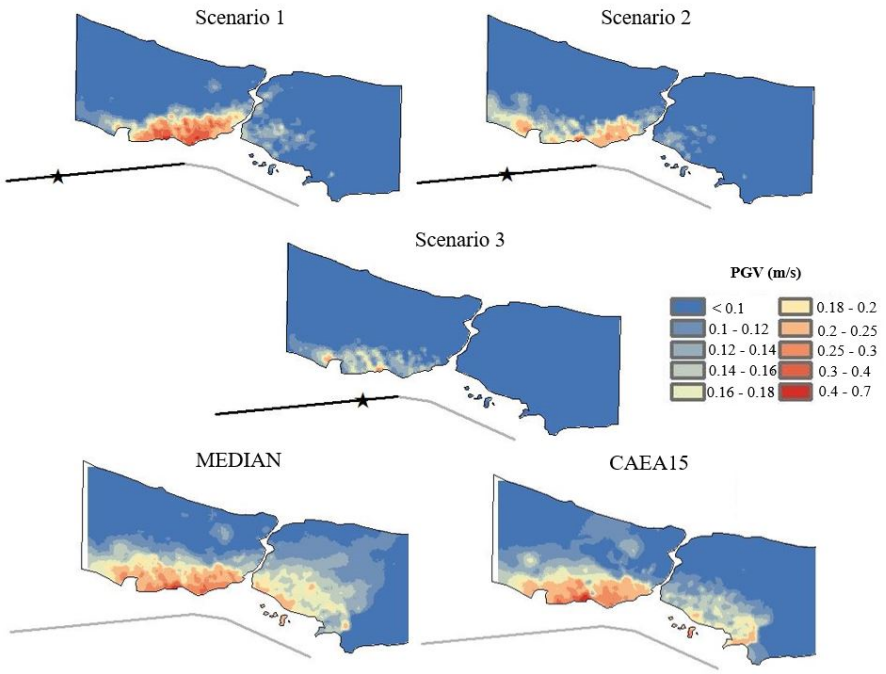

Fig. 9 Top: horizontal (geometric mean) PGV maps of the M_w7 scenarios considered in this work. Bottom: median PGV map based on all the 30 M_w7 scenarios (left) compared with the corresponding map based on the GMPE by Cauzzi *et al*. (2015) – CEA15.

How to take advantage of 3DPBNS in the framework of probabilistic seismic hazard assessment

In a nutshell, probabilistic seismic hazard assessment (PSHA) at a site can be set in the form

$$[IM > x] = \sum_{j=1,N} Prob\big[IM > x | scenario_j\big] Prob\big[scenario_j\big] \qquad (1)$$

where *IM* is a given ground motion intensity measure. In the classical PSHA, the *N* scenario earthquakes may occur throughout a seismic zone with annual probability $Prob[scenario_j]$ given by a frequency-Magnitude relationship set in the form

of the classical Gutenberg-Richter relationship, or other forms, including e.g. the characteristic earthquake model. The ground motion attenuation model is defined within the first factor at the right-hand side of eq. (1), and it is typically provided through a GMPE. Therefore, in the classical PSHA, eq. (1) is typically expressed in the form, referred for simplicity to a single seismic zone:

$$Prob[IM > x] = \iiint Prob[IM > x|m,r,\varepsilon] f_M(m) f_R(r) f_\varepsilon(\varepsilon) dm dr d\varepsilon \quad (2)$$

where $f(\cdot)$ denotes a probability density function, R is the distance from the site of a small area within the seismic zone where a magnitude M earthquake occurs, and ε is the spread of the GMPE.

In principle, moving from a GMPE-based to a 3DPBNS-based PSHA implies only the different evaluation of the term $Prob[IM>x|m,r,\varepsilon]$. In the first case, this term is computed based on the ergodic assumption that the probability distribution of *IM* can be obtained based on statistical evaluation of datasets of strong motion records from other regions of the world with similar tectonic framework. In the second case, it is computed by repetition of 3DPBNS of a given scenario earthquake at the site, in a number sufficient for a reliable evaluation of the probability distribution. For simplicity of notation, we will denote by *PSHAe* the *enhanced* seismic hazard assessment based on 3DPBNS.

Although *PSHAe* provides an obvious advantage to the standard GMPE, as already discussed in the Introduction, there are few examples in the literature of practical applications of such PSHAe (see e.g., Convertito *et al*., 2006; Graves *et al*., 2011; Villani *et al*., 2014), especially because of the large computational effort implied by computing the term *Prob [IM>x|scenario]*, extended to all potential scenarios, from low to large magnitude earthquakes.

For this reason, it is wise to limit application of the *PSHAe* to those contexts where seismic hazard is dominated by few near-source scenarios, for example a characteristic earthquake from a known seismic fault, with a relatively narrow range of possible magnitudes. The resulting framework for *PSHAe* may be set as in Figure 10, where GMPE-based and 3DPBNS-based PSHA are combined and applied selectively in their suitable ranges of magnitude.

Two different approaches may be envisaged for application of the *PSHAe*. With reference to Figure 11, the histograms at four sites in the Istanbul area are considered, showing the frequency distribution of computed PGV values according to 30 realizations through 3DPBNS of a M_w7 event along the North Anatolian Fault segment considered in this work. Frequency histograms are compared with the lognormal distribution, fit on the numerical results, as well as the corresponding distribution from two GMPEs (Cauzzi *et al*., 2015 – CEA15; Chiou and Youngs, 2008 – CHYO08).

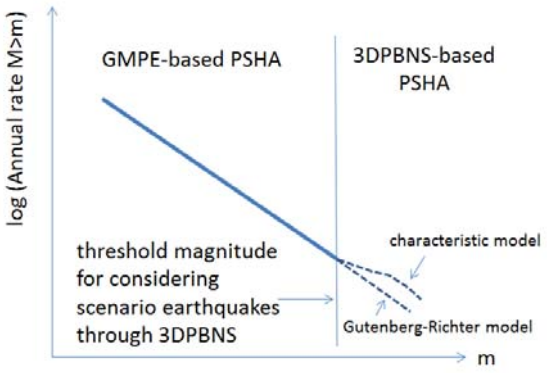

Fig. 10. A frequency-magnitude relationship explaining the range of applicability of different ground motion prediction models in the framework of an enhanced PSHA.

The first approach was called *high-resolution PSHA* by Villani *et al*. (2014) and consists, for the considered scenario earthquake, of replacing the moments of the lognormal distribution from the GMPE with those obtained from the 3DPBNS at each site of interest. This approach was implemented in the CRISIS software (Ordaz *et al*., 2013) through the so-called *generalized attenuation functions* (GAF). Of course, this *GAF-based PSHAe* is expected to provide different results from the GMPE-based PSHA, if the resulting probability distributions are significantly different.

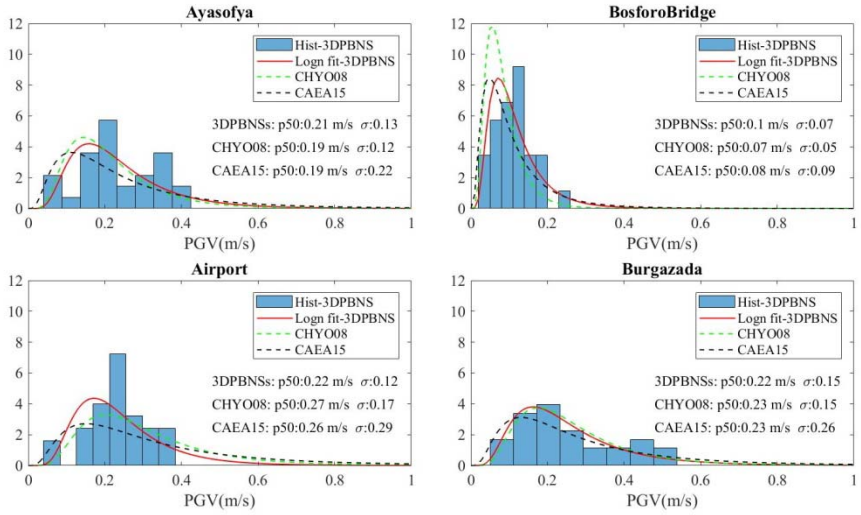

Fig. 11. Frequency histograms of simulated PGV for the 30 M_w7 earthquake ground motion scenarios simulated by SPEED at the 4 Istanbul sites considered in this study. Superimposed are the lognormal models based on the GMPEs by Cauzzi *et al* (2015) and Chiou and Youngs (2008).

However, comparing the frequency histograms with the probability density functions, it turns out that maximum PGVs from 3DPBNS are bounded, while those resulting from the extrapolation based on the probability model are not. This poses a well-known problem in the PSHA: whether or not bounded upper limits for the intensity ground motion measures should be placed in the PSHA (e.g., Abrahamson, 2000; Bommer *et al*., 2004; McGarr and Fletcher, 2007). Especially for the rare events implied by long return periods, integration along an unbounded range of variability of the ground motion parameters may provide in some cases very (and possibly unrealistically) conservative results. 3DPBNS may be helpful to provide site-specific limits for such upper bounds, if a sufficiently large set of realizations of the scenario is considered.

These arguments support consideration of a different approach for PSHAe, which takes full advantage of the 3DPBNS results, without postulating a probability model for ground motion. In this *footprint-based PSHAe* approach (Stupazzini *et al*. 2015), all realizations of the scenario earthquake are considered within a logic-tree framework, each with the same weight (Figure 12). This means that the probability distribution will be the same as provided by the frequency histogram, avoiding the extrapolation to assign non-zero probabilities to values of *IM* not resulting from the 3DPBNS. Furthermore, another potential added value of such an approach is that the spatial correlation structure of the results of PSHA is better maintained than with other approaches, since it does not suffer of the smoothing effects of the assumed probability model.

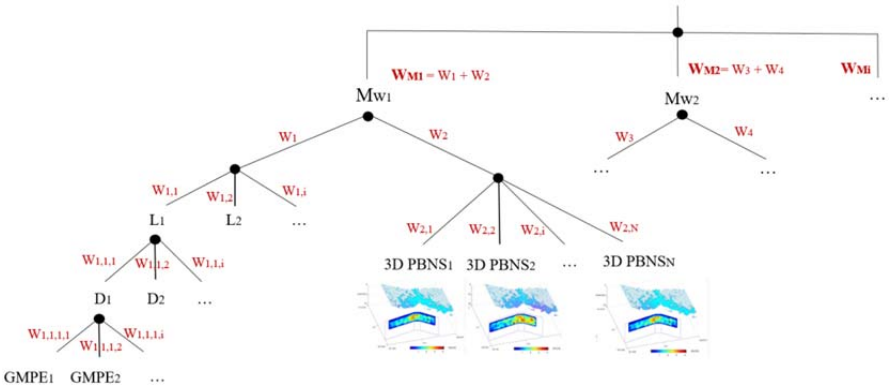

Fig. 12. Integration of the 3D PBNSs into a logic tree approach according to Stupazzini *et al*., 2015 (M_w: magnitude, L_j: location, D_j: depth, $GMPE_j$: ground motion prediction equation, 3D $PBNS_j$: 3D physics-based scenario, w_j: weight).

Figure 13 illustrates the results of the *footprint-based PSHAe* based only on 3D PBNSs (i.e. assigning zero weight to the GMPE branch, see Figure 12) in terms of horizontal (geometric mean) PGV hazard maps, for the return periods T_R = 475 and 975 years, compared with the corresponding hazard maps obtained using the GMPEs by Chiou and Youngs (2008), Cauzzi *et al*. (2015) and Bray and Rodri-

guez-Marek (2004). The latter was calibrated only adopting nearfield accelerograms presenting clear forward-directivity effects. Therefore, the predicted PGV tends to differ substantially from the prediction of Chiou and Youngs (2008) and Cauzzi *et al*. (2015). Another peculiar feature of the Bray and Rodriguez-Marek (2004) work, is that it distinguishes only between rock and soil and therefore it takes into account the variation of $V_{S,30}$ only up to a limited extent. This explains the more homogeneous maps obtained with this GMPE.

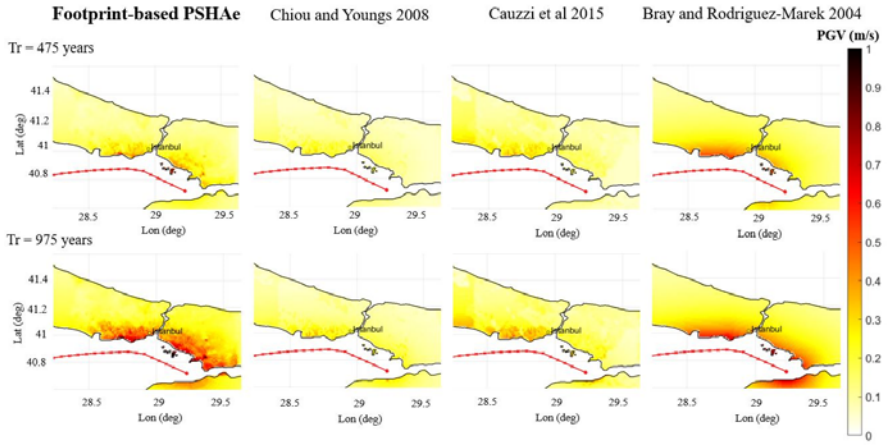

Fig. 13. Seismic Hazard Analysis based on 3D PBNSs, Chiou and Youngs (2008), Cauzzi *et al.* (2015), Bray and Rodriguez-Marek (2004) (from left to right). The hazard maps are presented in terms of PGV (m/s), geometric mean of the horizontal components, for T_R = 475 years (top) and 975 years (bottom).

It is worth noting that, for T_R = 475 years, the hazard map based on 3D PBNSs is lower than that obtained adopting Bray and Rodriguez-Marek (2004), while it agrees relatively well with the hazard map obtained using the other two GMPEs. On the contrary, for T_R = 975 years, the hazard map obtained adopting Bray and Rodriguez-Marek (2004) shows amplitudes of ground shaking similar to the hazard map produced by 3DPBNSs, while the two hazard maps based on the other GMPEs are systematically lower. As already mentioned and discussed in Infantino (2016), these results are due to the lack of back-directivity events of large magnitude (i.e. M_w 7.2 and 7.4), associated with the convex shape of the fault trace and its position with respect to the urban area of Istanbul, that controls the ground motion intensities for the longer return periods.

As already mentioned the footprint-based PSHAe is an extremely CPU intensive methodology and therefore the number of the 3DPBNSs to be simulated plays a crucial role in terms of its applicability. In the recent time we are exploring different strategies that seems to be quite promising in order to reduce the computational effort by wisely selecting “a priori” the 3DPBNSs and successively weighting them differently within our logic three.

Conclusions

"For a large earthquake, the epicenter is not as helpful for engineers as is the footprint" (Housner, 1999). With these words, one of the fathers of earthquake engineering commented the evidence from the August 17 1999 Turkish earthquake that the damage distribution could only be understood based on information of the dimensions of the faulted area and its position with respect to the site.

As a matter of fact, creating realistic realizations of future strong earthquake ground motions from known seismic faults and thus providing credible input motions for applications has been for long time a dream of engineering seismology. Within an application to future earthquake ground motions in Istanbul from the North Anatolian Fault branch crossing the Marmara Sea, we have shown in this paper the different and complicated steps involved, on the one side, in the creation of a fully 3D physics-based seismic model, and, on the other side, in the processing of numerical results and in their use for advanced applications of seismic hazard analyses.

Many of such steps are not fully resolved yet, but we have given in this paper some hints on how to cope effectively with them, within the intrinsic limitations of the 3DPBNS approach, but preserving its undeniable advantage over standard empirical approaches based on GMPEs.

More specifically, among the most important indications of this work, we list the following:

- even in the presence of an unlimited computer power and of a vast amount of knowledge, both on the seismotectonic, geological and geophysical context, the level of detail of available input data for 3DPBNS will be very hardly sufficient to solve frequencies larger than about 1.5 Hz: beyond this threshold, taking advantage of stochastic or hybrid methods is almost unavoidable;
- the proposed creation of broad-band synthetics based on an artificial neural network trained on strong motion records to provide a correlation between long and short period spectral ordinates seems to be an effective approach to create earthquake ground motion scenarios presenting a realistic spatial correlation structure and incorporating near-source and 3D site effects in a broad frequency range;
- to use results of 3DPBNS for seismic hazard analyses, a sufficient number of realizations is required to provide reliable distribution models to compute the probability of exceedance of given ground motion intensity measures (IMs): for this purpose, realistic random models for the kinematic co-seismic slip distribution along the fault should be provided;
- with respect to the GMPE-based approaches, the probability distribution models from 3DPBNS are expected to be more reliable, because they comply with the specific characteristics of the area.

Besides, it has been shown that the 3DPBNS approach allows one to avoid introducing in the PSHA a more or less arbitrary probabilistic model of the IM, with the well-known problem of assigning finite probabilities to extreme and unrealistic values of ground motion.

Acknowledgements

This work has been carried out in the framework of the 2014-2016 RELUIS RS2 Project funded by the Italian Department of Civil Protection as well as of research projects sponsored by industrial partners, namely, MunichRe (Germany) and swissnuclear (Switzerland). The third author of the paper, Ilario Mazzieri, has been partially supported by the Project "Modellazione numerica di fenomeni idro/geomeccanici per la simulazione di eventi sismici" funded by GNCS, Italy. The authors are grateful to Filippo Gatti for his contributions for the development of the ANN2BB tool.

References

Abrahamson NA (2000) State of practice of seismic hazard evaluation. In: Proc. GeoEng2000 Melbourne (Australia).

Akinci A, Aochi H, Herrero A et al (2017) Physics-Based Broadband Ground-Motion Simulations for Probable $M_w \geq 7.0$ Earthquakes in the Marmara Sea Region (Turkey). Bulletin of the Seismological Society of America 107: 1307-1323.

Ancheta TD, Darragh RB, Stewart JP et al (2014) PEER NGA-West2 database. Earthquake Spectra 30(3): 989-1005.

Aochi H, Douglas J, Ulrich T (2017) Stress accumulation in the Marmara Sea estimated through ground-motion simulations from dynamic rupture scenarios. Journal of Geophysical Research 122(3): 2219-2235.

Bohnhoff M, Bulit F, Dresen G et al (2013) An earthquake gap south of Istanbul. Nature communications 4 (1999).

Bommer JJ, Abrahamson NA, Strasser FO et al (2004) The challenge of defining upper bounds on earthquake ground motions. Seismological Research Letters 75(1): 82-95.

Boore DM (2003) Simulation of ground motion using the stochastic method. Pure and Applied Geophysics 160(3-4): 635-676.

Bray JD, Rodriguez-Marek A (2004) Characterization of forward-directivity ground motion in the near-fault region. Soil Dynamic and Earthquake Engineering, 24(11): 815-828.

Brune JN (1970) Tectonic stress and the spectra of seismic shear waves from earthquakes. Journal of Geophysical Research 75(26): 4997-5009.

Causse M, Chaljub E, Cotton F et al (2009) New approach for coupling k-2 and empirical Green's functions: application to the blind prediction of broad-band ground motion in the Grenoble basin. Geophysical Journal International 179(3): 1627-1644.

Cauzzi C, Faccioli E, Vanini M, Bianchini A (2015) Updated predictive equations for broadband (0.01-10 s) horizontal response spectra and peak ground motions, based on a global dataset of digital acceleration records. Bulletin of Earthquake Engineering 13(6): 1587-1612.

Chaljub E, Moczo P, Tsuno S et al (2010) Quantitative comparison of four numerical predictions of 3D ground motion in the Grenoble valley, France. Bulletin of the Seismological Society of America 100: 1427–1455.

Chiou BS-J, Youngs RR (2008) An NGA model for the average horizontal component of peak ground motion and response spectra. Earthquake Spectra 24(1): 173-215.

Convertito V, Emolo A, Zollo A (2006) Seismic-hazard assessment for a characteristic earthquake scenario: an integrated probabilistic-deterministic method. Bulletin of the Seismological Society of America 96(2): 377-391.

Crempien JGF, Archuleta RJ (2015) UCSB method for simulation of broadband ground motion from kinematic earthquake sources. Seismological Research Letters 86(1): 61-67.

Evangelista L, del Gaudio S, Smerzini C et al (2017) Physics-based seismic input for engineering applications: a case study in the Aterno river valley, Central Italy. Bulletin of Earthquake Engineering 15(7): 2645–2671.

Faccioli E, Maggio F, Paolucci R, Quarteroni A (1997) 2D and 3D elastic wave propagation by a pseudo-spectral domain decomposition method. Journal of Seismology, 1(3): 237-251.

Gallovič F, Brokešová J (2004) On strong ground motion synthesis with k-2 slip distributions. Journal of Seismology 8(2): 211-224.

Goulet CA, Abrahamson NA, Somerville PG, Wooddell KE (2015) The SCEC broadband platform validation exercise: methodology for code validation in the context of seismic-hazard analyses. Seismological Research Letters 86(1): 17-26.

Graves R, Jordan TH, Callaghan S et al (2011) CyberShake: a physics-based seismic hazard model for Southern California. Pure and Applied Geophysics 168(3-4): 367-381.

Guidotti R, Stupazzini M, Smerzini C et al (2011) Numerical study on the role of basin geometry and kinematic seismic source in 3D ground motion simulation of the 22 February 2011 M_w 6.2 Christchurch earthquake. Seismological Research Letters 82(6):767-782.

Herrero A, Bernard P (1994) A kinematic self-similar rupture process for earthquakes. Bulletin of the Seismological Society of America 84(4): 1216-1228.

Housner GW (1999) The footprint of an earthquake: opinion paper. Earthquake Spectra 15(4): 825.

Infantino M (2016) From 3D physics-based scenarios to advanced methods for seismic hazard assessment: the case of Istanbul. Master Thesis in Environmental Engineering. Politecnico di Milano.

Kamae K, Irikura K, Pitarka A (1998) A technique for simulating strong ground motion using hybrid Green's function. Bulletin of the Seismological Society of America 88(2): 357-367.

Madariaga R, Olsen KB (2002) Earthquake Dynamics. In: William Lee, Paul Jennings, Carl Kisslinger, Hiroo Kanamori (Eds) International Handbook of Earthquake & Engineering Seismology, Part A, Volume 81A, 1st edn., Academic Press.

Mai PM, Beroza GC (2003) A hybrid method for calculating near-source, broadband seismograms: application to strong ground motion prediction. Physics of the Earth and Planetary Interiors 137(1-4): 183-199.

Mai PM, Imperatori W, Olsen KB (2010) Hybrid broadband ground-motion simulations: combining long-period deterministic synthetics with high-frequency multiple S-to-S backscattering. Bulletin of the Seismological Society of America 100(5A): 2124-2142.

Mazzieri I, Stupazzini M, Guidotti R, Smerzini C (2013) SPEED: SPectral Elements in Elastodynamics with Discontinuous Galerkin: a non-conforming approach for 3D multi-scale problems. International Journal for Numerical Methods in Engineering 95(12): 991–1010.

McGarr A, Fletcher JB (2007) Near-fault peak ground velocity from earthquake and laboratory data. Bulletin of the Seismological Society of America 97(5): 1502-1510.

Motazedian D, Atkinson GM (2005) Stochastic finite-fault modeling based on dynamic corner frequency. Bulletin of the Seismological Society of America 95(3): 995-1010.

Ordaz M, Martinelli F, D'Amico V, Meletti C (2013) CRISIS2008: A flexible tool to perform seismic hazard assessment. Seismological Research Letters 84(3): 495-504.

Özgül N (2011) İstanbul il alanının jeolojisi. Yönetici özeti. Directorate of Earthquake And Geotechnical Investigation, Istanbul Metropolitan Municipality. http://ibb.gov.tr/tr-TR/SubSites/DepremSite/Pages/KentJeolojisiCalismalari.aspx/ İstanbul İl Alanının Jeolojisi Yönetici Özeti. Accessed 25 February 2015.

Paolucci R, Mazzieri I, Smerzini C, Stupazzini M (2014) Physics-based earthquake ground shaking scenarios in large urban areas. Perspectives on European Earthquake Engineering and Seismology. Chapter 10. Springer International Publishing, pp. 331-359.

Paolucci R, Mazzieri I, Smerzini C (2015). Anatomy of strong ground motion: near-source records and 3D physics-based numerical simulations of the M_w 6.0 May 29 2012 Po Plain earthquake, Italy. Geophysical Journal International 203(3): 2001–2020.

Paolucci R, Evangelista L, Mazzieri I, Schiappapietra E (2016) The 3D numerical simulation of near-source ground motion during the Marsica earthquake, central Italy, 100 years later. Soil Dynamics and Earthquake Engineering. 91: 39-52.

Paolucci R, Gatti F, Infantino M et al (2017) Broad-band ground motions from 3D physics-based numerical simulations using artificial neural networks. Bulletin of the Seismological Society of America (submitted for review).

Pilz M, Parolai S, Stupazzini M et al (2011) Modelling basin effects on earthquake ground motion in the Santiago de Chile basin by a spectral element code. Geophysical Journal International 187(2): 929–945.

Smerzini C, Villani M (2012) Broadband numerical simulations in complex near-field geological configurations: the case of the 2009 M_w 6.3 L'Aquila earthquake. Bulletin of the Seismological Society of America 102(6): 2436-2451.

Smerzini C, Galasso C, Iervolino I, Paolucci R (2014) Ground motion record selection based on broadband spectral compatibility. Earthquake Spectra 30(4): 1427-1448.

Stupazzini M, Paolucci R, Igel H (2009) Near-fault earthquake ground-motion simulation in the Grenoble Valley by a high-performance spectral element code. Bulletin of the Seismological Society of America, 99(1): 286-301.

Stupazzini M, Allmann A, Käser M et al (2015) PSHAe (Probabilistic Seismic Hazard Analysis enhanced): the case of Istanbul. In: Proceedings of the 10th Pacific Conference on Earthquake Engineering, Sydney, Australia.

Villani M, Faccioli E, Ordaz M, Stupazzini M (2014) High-resolution seismic hazard analysis in a complex geological configuration: the case of Sulmona Basin in Central Italy. Earthquake Spectra 30(4): 1801-1824.

MOX Technical Reports, last issues

Dipartimento di Matematica
Politecnico di Milano, Via Bonardi 9 - 20133 Milano (Italy)

67/2017 Esterhazy, S.; Schneider, F.; Mazzieri, I; Bokelmann, G.
Insights into the modeling of seismic waves for the detection of underground cavities

66/2017 Tamellini, M.; Parolini, N.; Verani, M.
An optimal control problem of two-phase compressible-incompressible flows

64/2017 Fumagalli, I.; Parolini, N.; Verani, M.
Optimal control in ink-jet printing via instantaneous control

65/2017 Regazzoni, F.;Parolini, N.;Verani M.
Topology optimization of multiple anisotropic materials, with application to self-assembling diblock copolymers

63/2017 Masci, C.; Paganoni, A.M.; Ieva, F.
Non-parametric mixed-effects models for unsupervised classification of Italian schools

62/2017 Barbarotta, L.; Rossi, S.; Dede', L.; Quarteroni, A.
A Transmurally Heterogeneous Orthotropic Activation Model for Ventricular Contraction and its Numerical Validation

61/2017 Vadacca, L.; Colciago, C. M.; Micheletti, S.; Scotti, A.
Three-dimensional fault representation by interface and solid elements: effects of the anisotropy of the fault zone permeability on the timing of triggered earthquakes

60/2017 Bonaldi, F.; Di Pietro, D. A.; Geymonat, G.; Krasucki, F.
A Hybrid High-Order method for Kirchhoff-Love plate bending problems

59/2017 Grujic, O.; Menafoglio, A.; Guang, Y.; Caers, J.
Cokriging for multivariate Hilbert space valued random fields. Application to multifidelity computer code emulation

58/2017 Landajuela, M.; Vergara, C.; Gerbi, A.; Dede', L.; Formaggia, L.; Quarteroni, A.
Numerical approximation of the electromechanical coupling in the left ventricle with inclusion of the Purkinje network